Electron-Vibration Coupling in Molecular Materials: Assignment of Vibronic Modes from Photoelectron Momentum Mapping

M. Graus,[1] M. Grimm,[1] C. Metzger,[1] M. Dauth,[2] C. Tusche,[3,4] J. Kirschner,[3] S. Kümmel,[2] A. Schöll,[1] and F. Reinert[1]

[1]*University of Würzburg, Experimental Physics VII, 97074 Würzburg, Germany*
[2]*University of Bayreuth, Theoretical Physics IV, 95440 Bayreuth, Germany*
[3]*Max Planck Institute of Microstructure Physics, 06120 Halle, Germany*
[4]*Peter Grünberg Institut (PGI-6), Forschungszentrum Jülich GmbH, 52425 Jülich, Germany*

(Received 5 February 2016; published 6 April 2016)

Electron-phonon coupling is one of the most fundamental effects in condensed matter physics. We here demonstrate that photoelectron momentum mapping can reveal and visualize the coupling between specific vibrational modes and electronic excitations. When imaging molecular orbitals with high energy resolution, the intensity patterns of photoelectrons of the vibronic sidebands of molecular states show characteristic changes due to the distortion of the molecular frame in the vibronically excited state. By comparison to simulations, an assignment of specific vibronic modes is possible, thus providing unique information on the coupling between electronic and vibronic excitation.

DOI: 10.1103/PhysRevLett.116.147601

The coupling of charge to vibronic excitation plays a crucial role for various physical phenomena from superconductivity [1–3] to the nonradiative decay pathways involved in photosynthesis [4]. In molecular materials, charge-vibration coupling influences the optical and electronic properties [5] and is a decisive quantity for the hopping transport [6–8]. In the case of hopping, the predominant transport mechanism for molecular solids relevant for device application [9], the charge mobility is immediately connected to the reorganization energy. The latter quantity is a measure of the energy cost for the deformation of the molecular frame upon adding or subtracting an electron. It has been demonstrated that photoelectron spectroscopy (PES) can be applied to quantify this reorganization energy from the analysis of the electron-vibration coupling from first principles [7,10].

The coupling of electronic to vibronic excitations has been studied for a long time by several methods such as PES [7,10,11], optical spectroscopy [12], x-ray absorption [13,14], and electron energy loss spectroscopy [15]. Nevertheless, an assignment of the specific vibrational modes that couple to the electronic excitation is complicated, since the experiment provides only information on the mode energy and restrictions on possible symmetries by selection rules.

Here we show that the angle-dependent intensity distribution in a PES experiment can provide a fingerprint of the coupled vibration. In the case of the paradigmatic molecule coronene [$C_{24}H_{12}$; see Fig. 3(c) for the molecular structure] investigated in this work, our analysis provides evidence that the mode which couples to an ionization of the highest occupied molecular orbital (HOMO) is an A_g in-plane mode with a vibronic excitation energy of 196 meV.

For our experiments the coronene molecules were prepared in a commensurate monolayer (ML) with 4×4 superstructure on an Au(111) substrate [16]. The interfacial bonding in this particular case is comparatively weak, thus leading only to a relatively small broadening of the molecular states due to hybridization with the metal. The momentum-resolved PES data were recorded at a sample temperature of 15 K and with He-I excitation (21.22 eV) utilizing a state-of-the-art photoelectron momentum microscope which collects all photoelectrons emitted into the complete half-sphere above the sample. This provides a three-dimensional data set of the photoemission spectral function $I(k_x, k_y, E_B)$, depending on the in-plane momentum coordinates (k_x, k_y) and the binding energy (E_B) with a momentum resolution of 0.005 Å^{-1} and energy resolution of 20 meV [17] (see Supplemental Material [18] for experimental details).

Figure 1(a) presents the energy distribution curve (EDC) derived from a data set recorded between the Fermi energy and the low-energy onset of the Au 5*d* band. The data were integrated over a circular area with diameter 0.5 Å^{-1} in momentum space centered at ($k_x = 1.45$ Å^{-1}; $k_y = 0$ Å^{-1}). The resulting spectrum shows a prominent peak at 1.5 eV, which can be assigned to the coronene HOMO. In addition, two shoulders appear on the high binding energy side, which resemble the equidistant vibronic overtones observed for several similar molecules in the gas and condensed phase [7,10].

For a detailed analysis of the fine structure of the coronene HOMO signal, shorter energy scans between 1.23 and 2.03 eV were performed to reduce the measurement time and radiation damage, which manifests itself in a

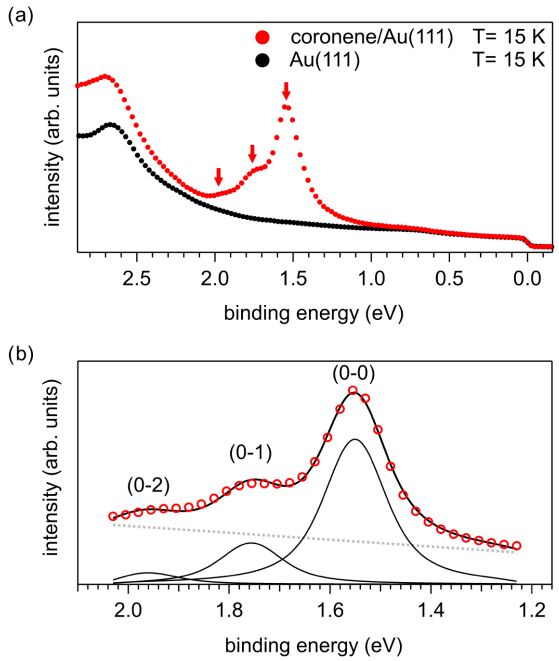

FIG. 1. (a) Momentum-integrated EDCs of 1 ML coronene on Au(111) recorded at a sample temperature of 15 K (red data points). The HOMO signal consists of three components (indicated by arrows). The corresponding data derived from a clean Au(111) sample considering the backfolding on the 4×4 superstructure of the adsorbate are plotted in black [see Fig. 2(d) and the corresponding text for details]. (b) Experimental spectrum derived from a short scan (red data points), fitted by a vibrational progression consisting of three equally spaced Voigt peaks of identical line width (black solid curves) and a linear background (black dotted line).

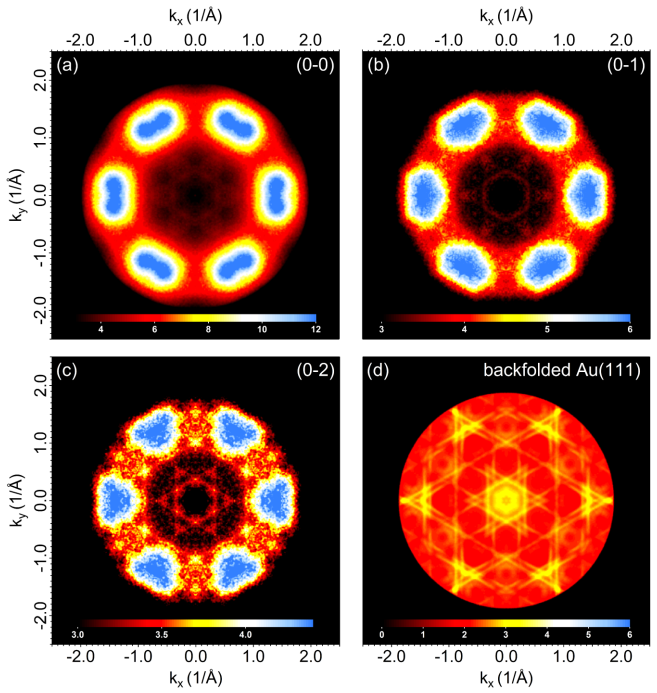

FIG. 2. (a)–(c) Photoelectron momentum maps of the HOMO of coronene/Au(111) recorded at the energy of the (0-0) peak and the vibronic sidebands (0-1) and (0-2). (d) Simulated background from the Au substrate derived by backfolding of a momentum map of a clean Au(111) sample (recorded at $E_B = 1.95$ eV; see Fig. S1 in Supplemental Material [18]) on the 4×4 superstructure of the adsorbate (see the text for details). The color scaling of the intensity was chosen individually to optimize the contrast.

broadening and slight energy shift of the molecular signals and the occurrence of additional low-energy features. With the applied settings, damage was visible after about 15 min of irradiation, while all data presented in the following were recorded in less than 10 min.

Figure 1(b) shows a spectrum derived from such a short scan after the same integration in momentum space as described above. To demonstrate the vibronic origin of the peaks on the high binding energy side, a least-squares fit was performed with three equidistant Voigt functions of equal width plus an additional linear background. The fit reproduces the experimental data well with Gaussian and Lorentzian widths of (79 ± 25) and (106 ± 25) meV, respectively, and an energy spacing of (206 ± 10) meV, representing the energy of the coupled vibration.

Figures 2(a)–2(c) show the photoelectron momentum maps recorded at a binding energy of 1.55, 1.75, and 1.95 eV, respectively, corresponding to the three individual vibronic peaks, which we will in the following refer to as (0-0), (0-1), and (0-2), respectively. (n-m) indicates a transition from the vibronic state n in the electronic ground state to the vibronic state m in the electronic excited state. No background subtraction was applied, and the color scale was adapted to enhance the color contrast of the individual patterns.

It has been demonstrated that the angle-dependent intensity distribution of photoelectrons is immediately connected to the electron density in real space [19,20]. In the case of planar organic molecules, a plane-wave final-state approximation of the photoemission final state allows furthermore a direct comparison of experimental momentum maps with calculated real-space orbitals by a Fourier transform [19,21]. In this sense, the intensity pattern recorded for the (0-0) peak in Fig. 2(a) resembles the previous experimental data for the HOMO of coronene on Ag(111) and the corresponding theoretical simulation for the coronene HOMO [22]. However, while the main features in the momentum map of the (0-0) peak appear oval or slightly goggle shaped, these features develop an increasing triangular appearance in case of the (0-1) and (0-2) peaks.

Since the peaks of (0-1) and particularly (0-2) have relatively low intensities, adapting the intensity scale in Figs. 2(b) and 2(c) results in an increasing contribution of emission from the substrate. To verify that the substrate signal does not interfere with the molecular features in the momentum maps, we have simulated the intensity patterns

derived from the Au sp bands taking into account the backfolding on the 4×4 superstructure of the adsorbate. For this purpose, a momentum map recorded at the same energy as the (0-2) peak for a clean Au(111) sample (see Fig. S1 in Supplemental Material [18]) was shifted by $1/4$, $2/4$, and $3/4$ of the $\bar{\Gamma} - \bar{\Gamma}$ distance towards each of the six adjacent surface-Brillouin zones and then averaged. The resulting intensity pattern is given in Fig. 2(d) and allows identifying the substrate signals in the momentum maps recorded for the (0-1) and (0-2) peaks of coronene/Au(111). The backfolded sp bands contribute relatively sharp patterns such as the two hexagrams, which are most clearly visible in the (0-2) momentum map [Fig. 2(c)]. Also, the slight increase in intensity around $k_x = 1.45$ Å^{-1}, $k_y = 0$ Å^{-1} and the intense lines along $k_x = 1.40$ Å^{-1} (and symmetrically equivalent sites) have to be associated with crossing points of multiple Au bands.

The comparison of the momentum patterns recorded for the low-intensity vibronic sidebands to the simulated background thus allows identification of several contributions from Au sp bands. Although some of these signals coincide with the intensity pattern from the coronene HOMO, the overall change of the coronene features towards a triangular shape cannot be explained by a contribution from the substrate.

The changes in Figs. 2(a)–2(c) thus obviously have to be sought in a change of the coronene electronic wave function in momentum—and thus also in real space—upon vibronic excitation. A deviation of the intensity patterns recorded for vibronically excited molecular states was already observed for pentacene [23] as well as for several phthalocyanines (X-Pc, $X =$ OTi, OV, ClAl, Pb, Cu, H_2) [24] and assigned to a breakdown of the sudden approximation in the photoionization process. In contrast to an instantaneous (vertical) transition, the photoemission process has to be rather described on a finite time scale, which is defined by the photohole lifetime. Photoemission thus bears information on a displacement of the nuclei on this very time scale.

Theoretical considerations can help to extract this information. Since the energy of the relevant vibrations is much larger than $k_B T$, the molecule is initially in its ground state [which is identical for the (0-0), (0-1), and (0-2) transitions]. Within the Born-Oppenheimer approximation, the electronic state of a system defines an energy surface, which acts as the potential for the motion of the nuclei. The change of the electronic potential that is caused by emission of an electron can trigger the vibronic excitation of the ionized system. While the common interpretation of angle-resolved PES based on ground-state single-particle orbitals can describe vertical processes well [19,25], it cannot capture structural changes of the molecular geometry caused by removing an electron. The latter, however, become accessible through the use of Dyson orbitals, defined by the projection of the $(N-1)$ electron ionized state $\Psi^+(N-1)$ onto the molecular ground state $\Psi_0(N)$ [20,26]:

$$\Psi_D = \sqrt{N}\langle \Psi_0(N) | \Psi^+(N-1) \rangle. \quad (1)$$

Viewing the PES process in terms of this overlap is ideally suited to our purpose, as the altering of the final molecular state's electronic structure due to the nucleis' vibrational displacement can easily be included explicitly. To identify possible vibrational modes, we perform a vibrational frequency analysis of positively charged isolated coronene using the density-functional theory with the Perdew-Burke-Ernzerhof exchange-correlation functional [27]. Nine modes are found in the energy range of interest between 185 and 250 meV (see Table I in Supplemental Material [18]). Since the vibronic excitations when time-averaged correspond to a displacement of the nuclei along normal coordinates, we calculated the electronic final state $\Psi^+(N-1)$ for displacement amplitudes ranging from zero up to a reasonable mean displacement of 0.15 Å [28]. In combination with the ground-state wave function of the neutral molecule, we evaluate the Dyson orbital according to Eq. (1) following the relaxed Slater determinant approach [20]. Approximating the photoelectron's state by a plane wave, which is justified for this class of materials [19,25], the photoelectron momentum maps can be simulated by a Fourier transform of the real-space Dyson orbitals into momentum space [20]. For the equilibrium position of the nuclei, i.e., the (0-0) transition, the corresponding momentum map is presented in Fig. 3(a) and resembles the single-particle molecular orbital case published earlier [22].

The overall agreement of Fig. 3(a) with its experimental counterpart in Fig. 2(a) is reasonable. However, the calculation does not reproduce the indicated goggle shape of the six main intensity maxima. Generally speaking, one possible explanation for this deviation could be a slight azimuthal tilt of the high-symmetry direction of coronene against the $[\bar{1}01]$ direction of the substrate surface. Taking into account different domains, this would lead to an azimuthal doubling of the intensity patterns in the experiment. However, based on such a multiplication of the calculated momentum map in Fig. 3(a), a simulation of the goggle features in Fig. 2(a) is not possible, thus rendering this explanation unlikely. An alternative explanation can be provided by the effect of lateral band dispersion. To reveal this, we have fitted the vibronic progression in the EDCs for all $k_\parallel$ in analogy to Fig. 1(b). The energy of the (0-0) peak derived from this fit shows a lateral dispersion of about 20 meV, which is a reasonable value compared to similar systems [29,30]. Moreover, when plotted against $k_\parallel$, the energy position of the (0-0) peak mimics the goggle shaped features in Fig. 2(a) (see Fig. S2 in Supplemental Material [18]). Since the experimental momentum maps were recorded at constant energy, energy dispersion of the

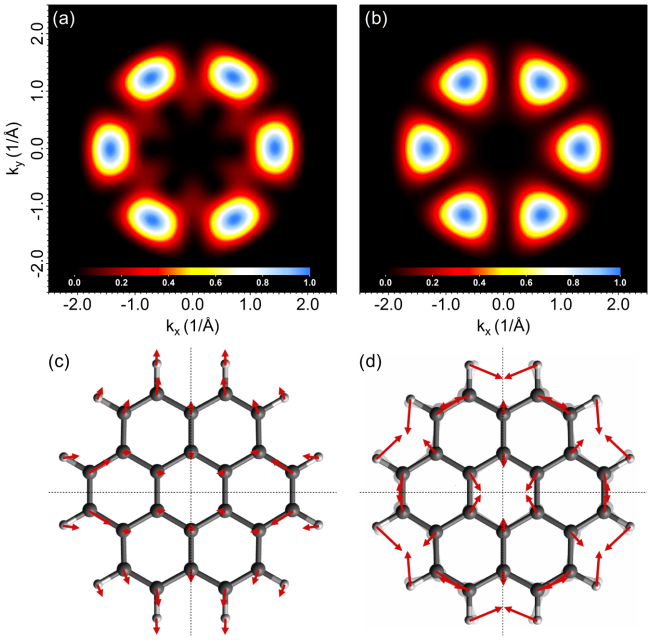

FIG. 3. Simulated photoelectron momentum maps derived for the Dyson orbital of (a) the coronene$^+$ HOMO with the nuclei in equilibrium position and (b) the HOMO of the distorted coronene$^+$ at a mean displacement amplitude of 0.15 Å according to the A_g mode at 196 meV. (c) Illustration of the geometric relaxation of an isolated coronene molecule upon ionization. The point group symmetry is reduced from D_{6h} to D_{2h}. Red arrows show the change in nuclear equilibrium positions enhanced by a factor of 50 for better visualization. The black dotted lines mark planes of symmetry, indicating an A_g symmetry of the distorted molecule. (d) Illustration of the respective A_g mode. The dark image indicates the undistorted molecule and is overlaid by a lighter image depicting the vibronic displacement. The associated force vectors are indicated as elongated red arrows.

(0-0) peak will directly translate to intensity variations, thus most likely accounting for the observed difference between the calculated and experimental momentum maps of the (0-0) peak.

For an increasing displacement of the nuclei, we find a change in the shape of the coronene features, depending on the displacement directions according to the individual vibrational modes. The momentum maps calculated for the nine vibrational modes between 180 and 250 meV at a mean displacement of 0.15 Å are depicted in Fig. S3 in Supplemental Material [18]. Interestingly, the modes show remarkable differences in the momentum maps. Only two modes show a change into a triangular pattern, which resembles the experimental finding for the vibronic sidebands in Figs. 2(a)–2(c).

Consequently, the changes in the photoemission data can be explained by changes of the molecular orbital density of the HOMO due to a deformation of the coronene molecule in a vibronically excited state. The gradual change from (0-0) over (0-1) to (0-2) is moreover plausible, since (0-1) to (0-2) represent transitions into different overtones of the same vibration, which have different mean displacement amplitudes. The simulation of the respective orbital density allows identifying the corresponding vibronic modes, a B_{2u} mode at 195 meV and an A_g mode at 196 meV, which fit quite well to the experimentally determined energy of (206 ± 10) meV. Moreover, the momentum patterns of the other modes in Fig. S3 obviously do not contribute significantly to the experimental data in Fig. 2, thus ruling out a coupling of these modes. This agrees with earlier studies that also found a preferential coupling of selected modes for pentacene and perfluoropentacene [31].

Based on our experimental data alone, we cannot derive further restrictions on the coupled vibronic modes. However, our calculations show that upon photoionization the coronene molecular frame relaxes as illustrated by Fig. 3(c), reducing the point group symmetry from D_{6h} to D_{2h}. The displacement of the nuclei is indicated by red arrows and shows A_g symmetry, thus resembling the A_g mode at 196 meV, which is depicted in Fig. 3(d) together with the corresponding momentum pattern in Fig. 3(b).

In summary, we demonstrated that the angle-dependent intensity patterns of photoelectrons of molecular states show characteristic changes due to the vibronic distortion of the molecule. By a comparison to the simulated patterns, an assignment of the specific vibronic modes that preferentially couple to the electronic excitation is possible. In the example of the coronene HOMO, the experimental data agree with two in-plane modes with an energy of 195 and 196 meV, respectively. The latter mode is A_g symmetric and should be favored according to symmetry arguments. Our approach of orbital imaging by photoelectron momentum mapping with high energy resolution thus provides unique information and constitutes a novel route for the analysis of the coupling between electronic and vibronic excitation and allows unprecedented insight into the properties of molecular materials.

A. S. and F. R. acknowledge support by the Deutsche Forschungsgemeinschaft (DFG; Grants No. GRK1221, No. SCHO-1260/4-1, No. SCHO-1260/5-1, and No. RE1469/9-1). M. D. and S. K. acknowledge support by DFG Graduiertenkolleg 1640 and the Bavarian State Ministry of Science, Research, and the Arts for the Collaborative Research Network "Solar Technologies go Hybrid." We thank J. Osterwalder, M. Hengsberger, and L. Castiglioni for fruitful discussion.

[1] A. Devos and M. Lannoo, Phys. Rev. B **58**, 8236 (1998).
[2] O. Gunnarsson, H. Handschuh, P. S. Bechthold, B. Kessler, G. Ganteför, and W. Eberhardt, Phys. Rev. Lett. **74**, 1875 (1995).
[3] T. Kato and T. Yamabe, J. Chem. Phys. **115**, 8592 (2001).
[4] T. Brixner, J. Stenger, H. Vaswani, M. Cho, R. Blankenship, and G. Fleming, Nature (London) **434**, 625 (2005).

[5] A. Mugarza, R. Robles, C. Krull, R. Korytár, N. Lorente, and P. Gambardella, Phys. Rev. B **85**, 155437 (2012).
[6] J. Brédas, J. Calbert, D. da Silva Filho, and J. Cornil, Proc. Natl. Acad. Sci. U.S.A. **99**, 5804 (2002).
[7] S. Kera, H. Yamane, and N. Ueno, Prog. Surf. Sci. **84**, 135 (2009).
[8] J. Sukegawa, C. Schubert, X. Zhu, H. Tsuji, D. Guldi, and E. Nakamura, Nat. Chem. **6**, 899 (2014).
[9] V. Coropceanu, J. Cornil, D. da Silva Filho, Y. Olivier, R. Silbey, and J. Brédas, Chem. Rev. **107**, 926 (2007).
[10] N. Ueno and S. Kera, Prog. Surf. Sci. **83**, 490 (2008).
[11] R. Boschi, J. N. Murrell, and W. Schmidt, Faraday Discuss. Chem. Soc. **54**, 116 (1972).
[12] D. Hudgins and L. Allamandola, J. Phys. Chem. **99**, 3033 (1995).
[13] A. Schöll, Y. Zou, L. Kilian, D. Hübner, D. Gador, C. Jung, S. G. Urquhart, T. Schmidt, R. Fink, and E. Umbach, Phys. Rev. Lett. **93**, 146406 (2004).
[14] A. Schöll, D. Hübner, T. Schmidt, S. Urquhart, R. Fink, and E. Umbach, Chem. Phys. Lett. **392**, 297 (2004).
[15] B. Koel, J. Crowell, C. Mate, and G. Somorjai, J. Phys. Chem. **88**, 1988 (1984).
[16] C. Seidel, R. Ellerbrake, L. Gross, and H. Fuchs, Phys. Rev. B **64**, 195418 (2001).
[17] C. Tusche, A. Krasyuk, and J. Kirschner, Ultramicroscopy **159**, 520 (2015).
[18] See Supplemental Material at http://link.aps.org/supplemental/10.1103/PhysRevLett.116.147601 for details on experiment and theory, experimental data on the back-folding of Au-bands, dispersion of the coronene HOMO, and the photoelectron momentum maps of the relevant vibronic modes.
[19] P. Puschnig, S. Berkebile, A. Fleming, G. Koller, K. Emtsev, T. Seyller, J. Riley, C. Ambrosch-Draxl, F. Netzer, and M. Ramsey, Science **326**, 702 (2009).
[20] M. Dauth, M. Wiessner, V. Feyer, A. Schöll, P. Puschnig, F. Reinert, and S. Kümmel, New J. Phys. **16**, 103005 (2014).
[21] J. Gadzuk, Phys. Rev. B **10**, 5030 (1974).
[22] M. Wießner, N. Lastra, J. Ziroff, F. Forster, P. Puschnig, L. Dössel, K. Müllen, A. Schöll, and F. Reinert, New J. Phys. **14**, 113008 (2012).
[23] H. Yamane, S. Nagamatsu, H. Fukagawa, S. Kera, R. Friedlein, K. K. Okudaira, and N. Ueno, Phys. Rev. B **72**, 153412 (2005).
[24] N. Ueno, S. Kera, K. Sakamoto, and K. Okudaira, Appl. Phys. A **92**, 495 (2008).
[25] M. Dauth, T. Körzdörfer, S. Kümmel, J. Ziroff, M. Wießner, A. Schöll, F. Reinert, M. Arita, and K. Shimada, Phys. Rev. Lett. **107**, 193002 (2011).
[26] M. Walter and H. Häkkinen, New J. Phys. **10**, 043018 (2008).
[27] J. P. Perdew, K. Burke, and M. Ernzerhof, Phys. Rev. Lett. **77**, 3865 (1996).
[28] G. Hagen and S. Cyvin, J. Phys. Chem. **72**, 1446 (1968).
[29] M. Wießner, J. Ziroff, F. Forster, M. Arita, K. Shimada, P. Puschnig, A. Schöll, and F. Reinert, Nat. Commun. **4**, 1514 (2013).
[30] M. Wießner, J. Kübert, V. Feyer, P. Puschnig, A. Schöll, and F. Reinert, Phys. Rev. B **88**, 075437 (2013).
[31] S. Kera, S. Hosoumi, K. Sato, H. Fukagawa, S. Nagamatsu, Y. Sakamoto, T. Suzuki, H. Huang, W. Chen, A. Wee, V. Coropceanu, and N. Ueno, J. Phys. Chem. C **117**, 22428 (2013).